

# Measuring $^{129}\text{Xe}$ transfer across the blood-brain barrier using MR spectroscopy

Madhwesha R. Rao   | Graham Norquay  | Neil J. Stewart  | Jim M. Wild 

POLARIS, Department of Infection, Immunity and Cardiovascular Disease and Insigneo Institute of In-silico Medicine, University of Sheffield, Sheffield, UK

## Correspondence

Madhwesha R. Rao, POLARIS, Department of Infection, Immunity and Cardiovascular Disease and Insigneo Institute of In-silico Medicine, University of Sheffield, POLARIS Building, 18 Claremont Crescent, Sheffield S10 2TA, UK.  
Email: m.rao@sheffield.ac.uk

## Funding information

Medical Research Council, Grant/Award Number: MRC - MR/M008894/1

**Purpose:** This study develops a tracer kinetic model of xenon uptake in the human brain to determine the transfer rate of inhaled hyperpolarized  $^{129}\text{Xe}$  from cerebral blood to gray matter that accounts for the effects of cerebral physiology, perfusion and magnetization dynamics. The  $^{129}\text{Xe}$  transfer rate is expressed using a tracer transfer coefficient, which estimates the quantity of *hyperpolarized*  $^{129}\text{Xe}$  dissolved in cerebral blood under exchange with *depolarized*  $^{129}\text{Xe}$  dissolved in gray matter under equilibrium of concentration.

**Theory and Methods:** Time-resolved MR spectra of hyperpolarized  $^{129}\text{Xe}$  dissolved in the human brain were acquired from three healthy volunteers. Acquired spectra were numerically fitted with five Lorentzian peaks in accordance with known  $^{129}\text{Xe}$  brain spectral peaks. The signal dynamics of spectral peaks for gray matter and red blood cells were quantified, and correction for the  $^{129}\text{Xe}$   $T_1$  dependence upon blood oxygenation was applied.  $^{129}\text{Xe}$  transfer dynamics determined from the ratio of the peaks for gray matter and red blood cells was numerically fitted with the developed tracer kinetic model.

**Results:** For all the acquired NMR spectra, the developed tracer kinetic model fitted the data with tracer transfer coefficients between 0.1 and 0.14.

**Conclusion:** In this study, a tracer kinetic model was developed and validated that estimates the transfer rate of HP  $^{129}\text{Xe}$  from cerebral blood to gray matter in the human brain.

## KEYWORDS

blood-brain barrier, gas-exchange, hyperpolarized xenon-129, time-resolved magnetic resonance spectroscopy, tracer kinetic model

## 1 | INTRODUCTION

The blood-brain barrier (BBB) separates the intravascular space from the brain parenchyma, and is formed by specialized endothelial cells held together by tight junctions,

covered by basal lamina and surrounded by pericytes, as shown in Figure 1. It acts as a selectively permeable barrier, which allows molecules essential for brain function through the barrier, while restricting the passage of noxious or neuroactive substances, and is vital for maintaining normal

This is an open access article under the terms of the Creative Commons Attribution License, which permits use, distribution and reproduction in any medium, provided the original work is properly cited.

© 2021 The Authors. *Magnetic Resonance in Medicine* published by Wiley Periodicals LLC on behalf of International Society for Magnetic Resonance in Medicine

neuronal function.<sup>1</sup> The consequence of a ruptured BBB is irregular transportation (and clearance) of gases, nutrients, water and other essential molecules across the barrier. These pathophysiological irregularities of an impaired BBB can be diagnostically assigned to various diseases processes,<sup>2-6</sup> typically by observing the movement of a tracer across the barrier. However, dysfunction of an intact BBB can also occur due to prolonged oxidative stress, causing deposition of plaque (example amyloid  $\beta$ ),<sup>7-9</sup> build-up of lipids, decline of pericytes,<sup>10</sup> cognitive ability and brain function.<sup>11</sup> This can occur even before the barrier becomes leaky or ruptured. For diagnosis, the two most commonly used tracers are iodinated contrast agent for X-ray CT and gadolinium chelated contrast agent for dynamic contrast enhanced MRI,<sup>12-16</sup> neither of which cross an intact BBB, but are able to when it is leaky or ruptured. The arterial spin labeling (ASL) based MRI technique<sup>17-21</sup> images magnetically tagged water molecules in the arterial blood delivered to brain tissue. Since the water molecules cross the *intact* BBB, this technique is being investigated for diagnosis of BBB diseases.<sup>22-24</sup> Nevertheless, the technique has some limitations due to acquisition strategy (post labeling delay time, labeling plane) competing with physiology (longitudinal relaxation time, arterial transit time) and abundance of water molecules in the brain tissue (background noise, magnetization transfer).<sup>19,25</sup>

Xenon is an exogenous tracer that passively crosses the *intact* BBB.<sup>1</sup> Recently, hyperpolarized (HP) xenon-129 has been demonstrated as an agent to image the uptake of inhaled gas into human brain tissue after crossing the *intact* BBB<sup>26,27</sup> by MRI, and the method has been shown to be

repeatable.<sup>28</sup> Preliminary clinical investigations of HP <sup>129</sup>Xe brain MRI have shown novel and complementary image contrast for stroke,<sup>29</sup> Alzheimer's disease<sup>30</sup> and functional brain imaging.<sup>31</sup> HP <sup>129</sup>Xe dissolved in the brain exhibits discrete chemical shifts for various biochemical compartments such as cerebral red blood cells (RBC), cerebrospinal/interstitial fluid, gray matter, white matter and soft muscular fat.<sup>27</sup> The image signal-to-noise ratio (SNR) and contrast is weighted by regional cerebral perfusion, physiology (tissue compartmental volumes, temperature, blood pressure) and gas-transfer from cerebral blood to gray matter across the BBB,<sup>26</sup> while the magnetization history of the HP <sup>129</sup>Xe during its journey through these compartments is also factorial.

The transfer dynamics of HP <sup>129</sup>Xe, a *passive* tracer, is not influenced by regional cellular metabolism, oxygen extraction<sup>32</sup> or electrolytic balance. Thus, HP <sup>129</sup>Xe MRI potentially holds unique information about the BBB by characterizing the *passive* transferability across the barrier. Nevertheless, this is influenced by the effects of regional brain physiology and perfusion. The HP aspect of the tracer adds further challenges as the MR detection is limited to the *HP* pool of <sup>129</sup>Xe,<sup>33</sup> but the gas transfer (membrane diffusion) dynamics are influenced by the concentration of all <sup>129</sup>Xe atoms in the respective compartments, some of which may not be HP and therefore are undetectable.

This study develops a tracer kinetic model to determine the transfer rate of HP <sup>129</sup>Xe from the cerebral blood to gray matter by considering the mass transfer of <sup>129</sup>Xe irrespective of its status of hyperpolarization, with the aim of quantitatively measuring the compartmental transfer dynamics in

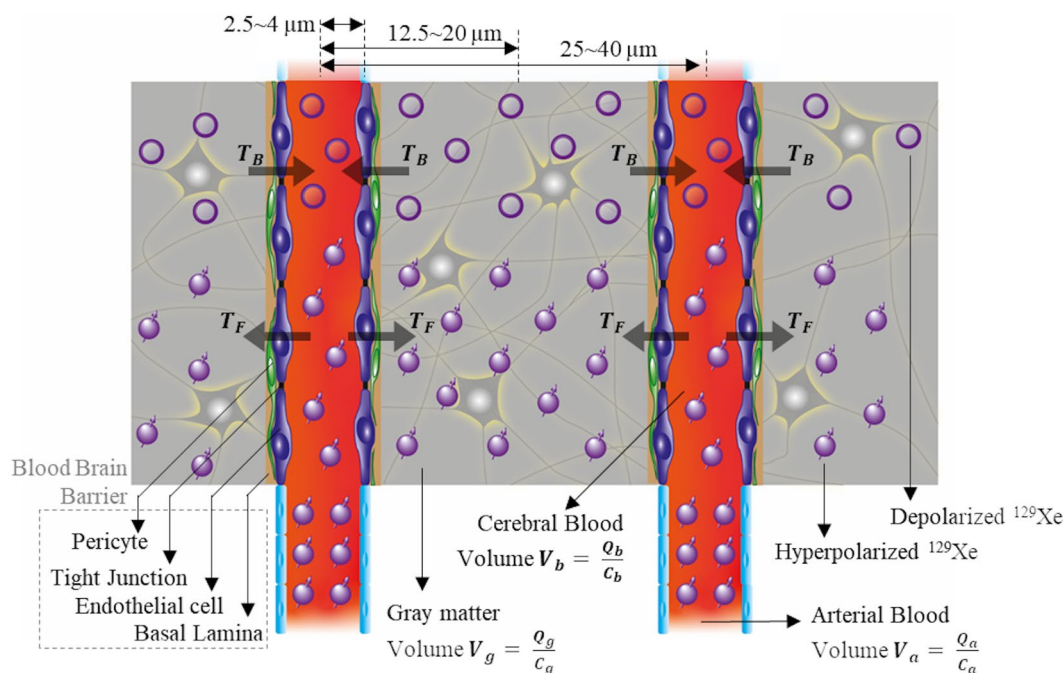


**FIGURE 1** Illustration of BBB, cerebral blood volume for gray matter, gray matter volume, arterial blood volume and transfer of xenon across the barrier

order to characterize the BBB function. In contrast to earlier mathematical modeling studies of  $^{129}\text{Xe}$  uptake in brain tissue that arrived at the concentration of  $^{129}\text{Xe}$  over time duration,<sup>34-36</sup> the model presented here uses the concentrations of  $^{129}\text{Xe}$  in cerebral blood and gray matter compartments measured using NMR spectroscopy to estimate the transfer dynamics between them. The proposed model also considers the variation in longitudinal relaxation of HP  $^{129}\text{Xe}$  dissolved in the blood by monitoring the variation in oxygenation-dependent chemical shift of RBC spectral peak.

## 2 | THEORY

### 2.1 | Tracer kinetic model for HP $^{129}\text{Xe}$ uptake in the brain

After inhalation of HP  $^{129}\text{Xe}$ , it crosses the alveolar-capillary barrier and is transported to the brain through the systemic circulation in approximately 4 s.<sup>37</sup> In the brain,  $^{129}\text{Xe}$  crosses the intact BBB passively in to the brain parenchyma,<sup>1</sup> and thereafter is under continuous diffusional exchange across the barrier. The cerebral blood volume of ~4 mL for 100 g of gray matter<sup>37-39</sup> and cerebral capillary of radius 2.5~4  $\mu\text{m}$ <sup>40-43</sup> implies that the radius of the gray matter coaxial with the capillary and mean distance between capillaries would be 12.5~20  $\mu\text{m}$  and 25~40  $\mu\text{m}$ <sup>40-43</sup> respectively, as shown in Figure 1. As the diffusion coefficient of xenon dissolved in the cerebral blood or gray matter has not been characterized, it can be approximated by using the diffusion coefficient dissolved in water of  $\sim 1 \times 10^{-5} \text{ cm}^2 \text{ s}^{-1}$ .<sup>44</sup> Under these conditions, a 95% equilibrium of concentration of  $^{129}\text{Xe}$  between cerebral blood and gray matter is reached in 0.2~0.4 seconds.<sup>45</sup> Hence, the NMR spectral peaks in time-resolved spectra that are acquired using a sequence repetition time (TR), that is longer than both the *cerebral mean transit time* ( $\approx 3.3 \text{ s}$ <sup>39,46,47</sup>) and *equilibrium time* (0.4 s), are linearly proportional to the concentration in the respective biochemical compartments.

Consider time-resolved NMR spectroscopic acquisitions where each acquisition consists of a RF excitation pulse and subsequent saturation pulses. After every acquisition the bulk magnetization of HP  $^{129}\text{Xe}$  is *depolarized* (DP) to thermal equilibrium such that the NMR signal from further excitation of this pool of  $^{129}\text{Xe}$  in the brain is too weak to be detectable. Therefore, in each of the acquired time-resolved spectra, the spectral peaks do not represent the total quantity; instead, they represent the quantity of HP  $^{129}\text{Xe}$  accumulated between two consecutive NMR acquisitions. Nevertheless, there is continuous accumulation of DP  $^{129}\text{Xe}$  in the brain. Due to their respective discrete chemical shifts,<sup>27</sup> the change in the relative concentration of HP  $^{129}\text{Xe}$  in cerebral blood and gray matter can be monitored over time, and thus HP  $^{129}\text{Xe}$  can be

used as a tracer to examine the transfer dynamics across the shared barrier. Because there is a continuous arterial in-flow of HP  $^{129}\text{Xe}$  to the cerebral vasculature, the *forward transfer* ( $T_F$ ) of  $^{129}\text{Xe}$  from cerebral blood to gray matter is HP  $^{129}\text{Xe}$  and therefore is detectable, annotated as  $T_F$  in Figure 1. We define the  $T_F$  rate as the quantity of HP  $^{129}\text{Xe}$  delivered to gray matter in the time duration (TR) between two successive acquisitions, considering both arterial in-flow of HP  $^{129}\text{Xe}$  and diffusional gas-exchange across the BBB. Due to the radiofrequency (RF) saturation pulses used after each acquisition, the *backward transfer* of  $^{129}\text{Xe}$  from gray matter to cerebral blood is DP  $^{129}\text{Xe}$  and therefore is undetectable, annotated as  $T_B$  in Figure 1. NMR detection depends on the magnetization ( $M$ ), which is proportional to the quantity ( $Q$ ) and polarization of  $^{129}\text{Xe}$ , whereas the transfer dynamics depends on concentration ( $C$ ), which is proportional to the quantity irrespective of its status of polarization.

For a given cerebral blood flow for gray matter  $F$ , partition coefficient of xenon between gray matter and blood  $\lambda$ , cerebral mean transit time  $\psi$ , cerebral blood volume  $V_{\text{Blood}}$  per volume of gray matter  $V_{\text{GM}}$ , concentration of HP  $^{129}\text{Xe}$  in arterial blood  $C_A$  and NMR spectral repetition time  $t_{\text{TR}}$ , using Fick's principle developed for an inert gas tracer by Kety,<sup>45</sup> we can arrive at the concentration of  $^{129}\text{Xe}$  in gray matter  $C_{\text{GM}}$  for the time instance immediately after the  $(n-1)^{\text{th}}$  RF acquisition as shown in Equation (1); nevertheless, this pool of  $^{129}\text{Xe}$  would be DP  $^{129}\text{Xe}$ .

$$C_{\text{GM},\text{DP}} = \lambda C_A \left( 1 - e^{-\frac{t_{\text{TR}}(n-1)}{V\psi}} \right) \quad (1)$$

where,  $F\lambda^{-1}V_{\text{GM}}^{-1} = V_{\text{Blood}}\lambda^{-1}V_{\text{GM}}^{-1}\Psi^{-1} = V^{-1}\Psi^{-1}$  and  $V^{-1} = V_{\text{Blood}}\lambda^{-1}V_{\text{GM}}^{-1}$ . The quantities of HP ( $Q_{\text{GM},\text{HP}}$ ) and DP ( $Q_{\text{GM},\text{DP}}$ )  $^{129}\text{Xe}$  in the gray matter at the time instance at the  $n^{\text{th}}$  RF acquisition are:

$$Q_{\text{GM},\text{HP}} = \lambda V_{\text{GM}} C_A \left( 1 - e^{-\frac{t_{\text{TR}}}{V\psi}} \right) \quad (2)$$

$$Q_{\text{GM},\text{DP}} = \lambda V_{\text{GM}} C_A \left( 1 - e^{-\frac{t_{\text{TR}}(n-1)}{V\psi}} \right)$$

Such that, the total quantity of xenon is  $Q_{\text{GM}} = Q_{\text{GM},\text{HP}} + Q_{\text{GM},\text{DP}}$ . Between the time instances of the  $(n-1)^{\text{th}}$  and  $n^{\text{th}}$  RF acquisition, there is continuous diffusional exchange of  $^{129}\text{Xe}$  between gray matter and cerebral blood. If we let  $r$  be the fraction of  $^{129}\text{Xe}$  in gray matter that would exchange with  $^{129}\text{Xe}$  in cerebral blood, we have  $Q_{\text{GM}} = (1-r)Q_{\text{GM}} + rQ_{\text{GM}}$ , where  $rQ_{\text{GM}}$  is the quantity of  $^{129}\text{Xe}$  that would exchange with cerebral blood. Further, because we have two pools of  $^{129}\text{Xe}$  (HP and DP) in both gray matter and cerebral blood, for the fraction of  $^{129}\text{Xe}$  that would exchange with cerebral blood, we have four possibilities of

exchange: (i) HP  $^{129}\text{Xe}$  being replaced by HP  $^{129}\text{Xe}$   $Q_{GM,HP \leftrightarrow HP}$ , (ii) HP  $^{129}\text{Xe}$  being replaced by DP  $^{129}\text{Xe}$   $Q_{GM,HP \leftrightarrow DP}$ , (iii) DP  $^{129}\text{Xe}$  being replaced by DP  $^{129}\text{Xe}$   $Q_{GM,DP \leftrightarrow DP}$ , and (iv) DP  $^{129}\text{Xe}$  being replaced by HP  $^{129}\text{Xe}$   $Q_{GM,DP \leftrightarrow HP}$ . Letting  $k_1$  and  $k_2$  be the factors that determine the fraction of  $^{129}\text{Xe}$  of a particular pool being replaced by the same pool, we can then derive the six-term expression;

$$Q_{GM} = (1-r) (Q_{GM,HP} + Q_{GM,DP}) + r (k_1 Q_{GM,HP \leftrightarrow HP} + (1-k_1) Q_{GM,HP \leftrightarrow DP} + k_2 Q_{GM,DP \leftrightarrow DP} + (1-k_2) Q_{GM,DP \leftrightarrow HP}) \quad (3)$$

The factors  $(1-k_1)$  and  $(1-k_2)$  are the tracer transfer constants that determine the fraction of one pool of  $^{129}\text{Xe}$  being replaced by the other pool. For simplicity of calculation in the current context, we use;  $k=k_1=k_2$ . In Equation (3), only the first, third and last term relate to HP  $^{129}\text{Xe}$  which contributes to the NMR signal, thus rewriting and substituting from Equation (2), we have;

$$Q_{GM,HP} = \lambda V_{GM} C_A \left[ (1-r(1-k)) \left( 1 - e^{-\frac{t_{TR}}{T_2^*}} \right) + r(1-k) \left( 1 - e^{-\frac{t_{TR}(n-1)}{T_2^*}} \right) \right] \quad (4)$$

Equation (4) assumes that the gray matter compartment is solely in exchange with the cerebral blood compartment, and vice versa. The factor  $r$  that determines the fraction of  $^{129}\text{Xe}$  that would exchange with cerebral blood depends on several factors such as the capillary diameter, the mean distance between capillaries and the diffusivity of  $^{129}\text{Xe}$ . Consider the diffusivity of  $^{129}\text{Xe}$  in water  $D = 1 \times 10^3 \mu\text{m}^2\text{s}^{-1}$  and the mean diffusive displacement from gray matter volume to cerebral blood volume  $d_{GM \rightarrow Blood} \approx 12.5 \sim 20 \mu\text{m}$  from Figure 1,<sup>40-43</sup> the time taken ( $t_{GM \rightarrow Blood}$ ) for diffusion from gray matter to cerebral blood volume is approximately;

$$t_{GM \rightarrow Blood} = \frac{1}{2} d_{GM \rightarrow Blood}^2 D^{-1} \approx 75 \sim 200 \text{ ms}$$

Thus, the factor  $r$  can be approximated as;

$$r = \begin{cases} 1 & \forall (t_{TR} - \psi) t_{GM \rightarrow Blood}^{-1} > 1 \\ (t_{TR} - \psi) t_{GM \rightarrow Blood}^{-1} & \forall 1 > (t_{TR} - \psi) t_{GM \rightarrow Blood}^{-1} > 0 \\ 0 & \forall 0 > (t_{TR} - \psi) t_{GM \rightarrow Blood}^{-1} \end{cases}$$

For the quantity of HP  $^{129}\text{Xe}$  in cerebral blood,  $Q_{Blood,HP}$ , we have  $\frac{dC_{Blood,HP}}{dt} = \frac{F}{\lambda V_{GM}} C_A$ , where  $C_{Blood,HP}$  is the concentration of HP  $^{129}\text{Xe}$  in cerebral blood. Rearranging and integrating for the time interval  $t_{TR}$ , we have;  $C_{Blood,HP} = \frac{t_{TR}}{V_{\Psi}} C_A$ , and  $Q_{Blood,HP}$  as;

$$Q_{Blood,HP} = \frac{t_{TR}}{V_{\Psi}} V_{Blood} C_A \quad (5)$$

Similarly, for the quantity of HP  $^{129}\text{Xe}$  in arterial blood  $Q_{A,HP}$ ,  $Q_{A,HP} = C_A V_A$ , where  $V_A$  is the arterial blood volume between the lungs and the brain.

To corroborate tracer kinetics with the detected NMR spectroscopy, let  $M_0$  be the bulk magnetization, such that  $M_0 \approx QP\Phi$ , where  $Q$  is the quantity of  $^{129}\text{Xe}$  and  $\Phi$  depends on gyromagnetic ratio, reduced Planck's constant and nuclear spin quantum number.<sup>48</sup>  $P$  is the polarization of the sample, such that  $P_{HP}$  and  $P_{DP}$  are the polarization of the HP pool of  $^{129}\text{Xe}$  that is detectable and DP pool of  $^{129}\text{Xe}$  that is not detectable respectively. The magnetization in transverse plane is propositional to  $M_0$ , weighted by flip angle and transverse relaxation time ( $T_2^*$ ). For a  $90^\circ$  flip angle, the acquired NMR signal is given by  $M_0 e^{j2\pi f_0 t} e^{-\frac{t}{T_2^*}}$ , where  $f_0$  is the center frequency of the spectral peak. The corresponding Fourier transform is given by  $M_0 \left( (T_2^*)^{-1} + j2\pi(f_0 - f) \right)^{-1}$ ,<sup>49</sup> which is a Lorentzian function  $L\{\delta, f\}$  if we let  $T_2^* = (\pi\delta)^{-1}$ , where  $\delta$  is the half power peak width. Further, integrating the spectrum, we have  $M_0 \int_{-\infty}^{\infty} L\{\delta, f\} = M_0$ , and thus, the magnitude of the spectral peak ( $M_{GM}, M_{Blood}$ ) measures the quantity ( $Q_{GM}, Q_{Blood}$ ) of  $^{129}\text{Xe}$  for a given polarization.  $P_{DP}$  depends on the strength of the static magnetic field, Boltzmann's constant, gyromagnetic ratio, reduced Planck's constant and temperature of  $^{129}\text{Xe}$ .<sup>48</sup>  $P_{HP}$  depends on the polarization achieved by the spin-exchange optical pumping process and  $P_{HP} \approx P_{DP} 10^5$ .<sup>33</sup> The polarization ( $P_{HP}$ ) decays by longitudinal relaxation in several distinct biochemical compartments on its journey to the brain; in the gas-phase in the lungs  $T_{1,GAS}$ , in the dissolved-phase in the blood  $T_{1,Blood,L \rightarrow B}$  during the lung-to-brain ( $L \rightarrow B$ ) transit time  $\tau_{L \rightarrow B}$  and in the dissolved-phase in the gray matter  $T_{1,GM}$  during the TR ( $t_{TR}$ ). Considering the decay of polarization, for a detectable NMR spectral peak at the  $n^{th}$  acquisition, we have the longitudinal magnetization as:

$$M_A = \Phi P_{HP} \Gamma Q_{A,HP} e^{-\frac{t_{TR}^n}{T_{1,GAS}}} e^{-\frac{\tau_{L \rightarrow B}}{T_{1,Blood,L \rightarrow B}}} \quad (6)$$

$$M_{Blood} = \Phi P_{HP} b_{RBC} Q_{Blood,HP} e^{-\frac{t_{TR}}{T_{1,Blood}}}$$

$$M_{GM} = \Phi P_{HP} Q_{GM,HP} e^{-\frac{t_{TR}}{T_{1,GM}}}$$

where,  $b_{RBC}$  is a scalar factor determining the quantity of  $^{129}\text{Xe}$  in the RBCs in the whole of the head when compared to the total quantity of  $^{129}\text{Xe}$  in cerebral blood that is in exchange with gray matter.  $\Gamma$  is a factor defining the dynamics of  $^{129}\text{Xe}$  signal in the lungs, such as exchange rate across the

alveolar-capillary barrier and the relative volumes/pressure of alveoli and Pulmonary capillaries. Considering the ratio of  $M_{GM}$  by  $M_{Blood}$  and rearranging the terms, we have:

$$\frac{M_{GM}}{M_{Blood}} = \frac{Q_{GM,HP}}{e^{-\frac{t_{TR}}{T_{1Blood}}}} \left( \frac{e^{-\frac{t_{TR}}{T_{1GM}}}}{b_{RBC} Q_{Blood,HP}} \right) \quad (7)$$

Equation (7) is the tracer kinetic model for transfer dynamics of  $HP^{129}\text{Xe}$  in the brain and is the estimate of the forward transfer  $T_F$  rate in Figure 1. The transfer dynamic is independent of  $Q_{A,NMR}$  and the term in the brackets in Equation (7) is a constant. Although  $-\frac{t_{TR}}{T_{1Blood}}$  is independent of time,  $T_{1Blood}$  varies with the oxygenation of cerebral blood. Nevertheless, this dependence of  $T_{1Blood}$  is well established in the literature and the chemical shift of the RBC spectral peak can be used to monitor variations in blood oxygenation and apply a  $T_1$  correction accordingly.<sup>32,50-52</sup> Table 1 provides a list of the various parameters used in the study.

### 3 | METHODS

In vivo MR brain spectroscopy with  $^{129}\text{Xe}$  was performed with approval from the UK National Research Ethics Committee. Spectroscopic experiments were conducted on three healthy male volunteers aged 25 y, 33 y and 34 y, and repeated three times for each of the volunteers. The heart rate and  $\text{SO}_2$  were monitored throughout the breath hold, which lasted no more than 24 s.

Experiments were performed on a GE HDx 1.5 T clinical MRI scanner.  $^{129}\text{Xe}$  gas was HP to  $P_{HP} > 30\%$  polarization using a POLARIS (Sheffield, UK) regulatory approved spin

exchange optical pumping polarizer.<sup>53</sup> HP  $^{129}\text{Xe}$  gas of 500 mL was mixed with  $\text{N}_2$  for a total inhaled dose of 1 L. An eight-leg band-pass birdcage RF coil was used<sup>27</sup> for transceiver; with inner diameter of 300 mm and length of 295 mm. The gas mixture was administered by inhalation from a Tedlar bag as described in Rao et al.<sup>26</sup> Time-resolved whole-brain spectra were acquired during a breath-hold, so that the HP  $^{129}\text{Xe}$  gas mixture was maintained as a reservoir in the lungs supplying the dissolved  $^{129}\text{Xe}$  plasma and RBC signal to the brain through alveolar-capillary gas exchange and onward through the systemic circulation.

MR spectroscopy parameters were as follows: center frequency = 17660800 Hz (198 ppm downfield from the  $^{129}\text{Xe}$  gas phase resonance), flip angle =  $90^\circ$ , non-selective RF hard-pulse with duration of 500  $\mu\text{s}$ , receiver bandwidth = 1.2 kHz and number of sample points = 128. The acquisition time was  $\sim 107$  ms, much longer than  $T_2^*$  of  $^{129}\text{Xe}$  in RBC (2 ms<sup>54</sup>) and gray matter (8.8 ms<sup>27</sup>). TR was set to 4 s, which is longer than the typical cerebral mean transit time ( $\Psi$ ) of 3.3 s<sup>39,46,47</sup> and the equilibrium time of 0.4 s,<sup>45</sup> assuming  $\Psi$  will not increase by more than 20% during the breath-hold.<sup>55</sup> Acquisition of time-resolved spectra was initiated immediately after the inhalation of the gas dose with two cycles of non-selective  $90^\circ$  RF pulses to destroy the polarization of the initial unknown quantity of HP  $^{129}\text{Xe}$  in the brain. After each subsequent pulse-acquire NMR spectroscopic acquisition, two non-selective  $90^\circ$  RF pulses were applied to destroy the polarization of the residual HP  $^{129}\text{Xe}$ .

A summation of five complex Lorentzian peaks in accordance with the known five spectral peaks of  $^{129}\text{Xe}$  dissolved in the human head<sup>27,36</sup> was numerically fitted to the acquired NMR spectra, and each of the spectral peaks were quantified as a product of  $\pi$ , height and width of the peak. These quantified

**TABLE 1** List of key parameters used for the tracer kinetic model and analysis

Parameter	Symbol	Value	Reference
Cerebral blood volume for 100 g of gray matter $V_{GM}$	$V_{Blood}$	$\sim 4$ mL	37-39
Radius of cerebral capillaries	–	2.5 ~ 4 $\mu\text{m}$	40-43
Mean distance between capillaries	–	25 ~ 40 $\mu\text{m}$	40-43
Diffusion coefficient of $^{129}\text{Xe}$ dissolved in water	$D$	$1 \times 10^3 \mu\text{m}^2 \text{s}^{-1}$	44
Time to reach 95% equilibrium in concentration	–	0.2 ~ 0.4 s	45
$^{129}\text{Xe}$ Partition coefficient gray matter/blood	$\lambda$	0.88	56
Cerebral mean transit time	$\psi$	3.3 s	39,46,47
Longitudinal relaxation of $^{129}\text{Xe}$ in blood	$T_{1Blood}$	4.5 s	32,50-52
Transverse relaxation of $^{129}\text{Xe}$ in blood	–	2 ms	54
Transverse relaxation of $^{129}\text{Xe}$ in gray matter	–	8.8 ms	27
Factor $r$	$r$	1	This study
$^{129}\text{Xe}$ displacement time	$t_{GM \rightarrow Blood}$	75 ~ 200 ms	This study
Repetition Time (TR)	$t_{TR}$	4 s	This study

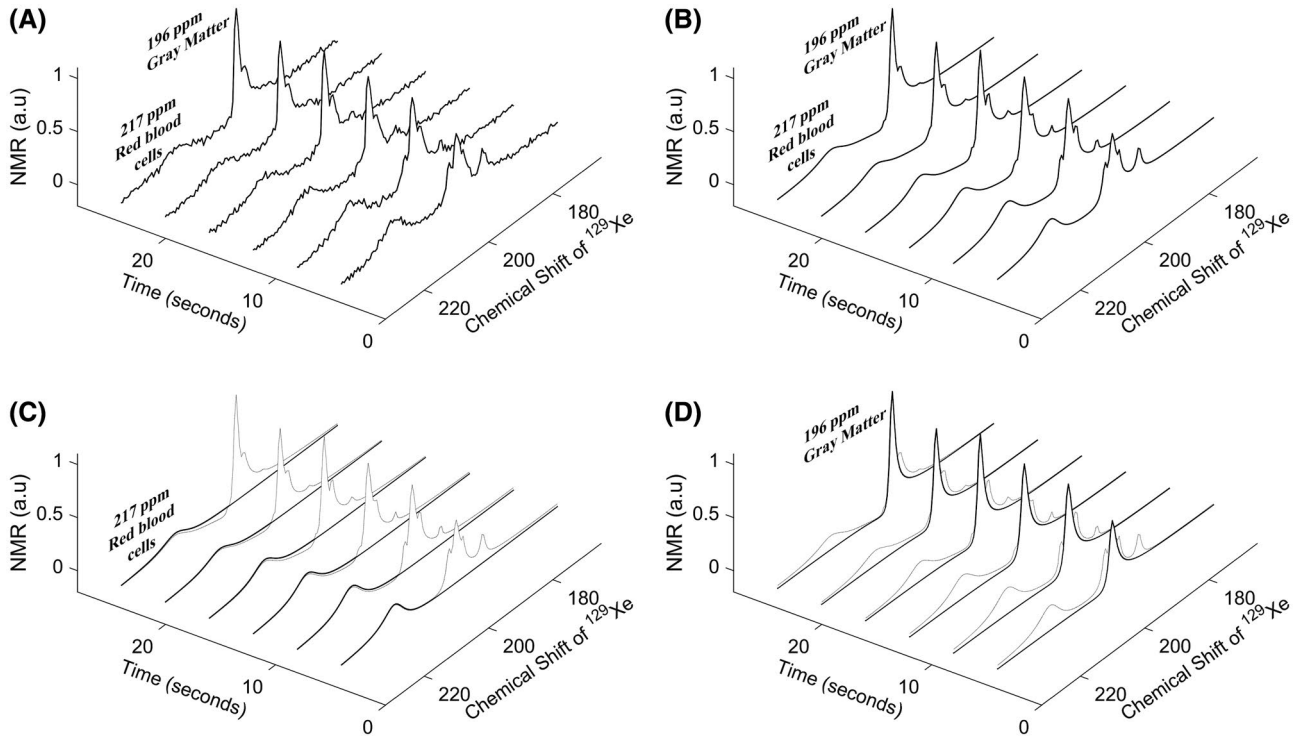


**FIGURE 2** A, Acquired spectra for volunteer 34 y old, male. B, Artificially generated spectra comprising five complex Lorentzian peaks to numerically fit the acquired spectra in (A). Artificially generated complex Lorentzian peak for cerebral red blood cells (C) and gray matter (D)

spectral peaks represent the bulk magnetization of  $^{129}\text{Xe}$  in corresponding compartments, namely  $M_{GM}$  and  $M_{Blood}$  for gray matter and cerebral RBC compartments, respectively.

The transfer dynamics of  $^{129}\text{Xe}$  between gray matter and cerebral blood was determined by evaluating the ratio of the time course of the spectral peaks of  $^{129}\text{Xe}$  in gray matter and cerebral RBC ( $M_{GM}M_{Blood}^{-1}$ ). Using typical physiological values; cerebral blood volume for gray matter of 4 mL per 100 g of tissue,<sup>37-39</sup> cerebral mean transit time of 3.3 s<sup>39,46,47</sup> and the partition coefficient for xenon dissolved in gray matter to blood as 0.88<sup>56</sup> (see Table 1); the tracer kinetic model in Equation (7) was rescaled and numerically fitted to the acquired transfer dynamics using a range of tracer transfer constants  $(1 - k) = 0$  to 1. The error in the numerical fit was calculated as the standard deviation of the difference between the tracer kinetic model from Equation (7) and the acquired transfer dynamic ratio, expressed as a percentage by normalizing by the mean value of the acquired transfer dynamic ratio.

## 4 | RESULTS

A typical series of time-resolved spectra acquired from the head of the 34-y-old male volunteer is shown in Figure 2A. Summation of five complex Lorentzian peaks fitted to the

acquired spectrum in Figure 2A is shown in Figure 2B. The time course of the individual spectral peaks of  $^{129}\text{Xe}$  dissolved in cerebral RBC and gray matter is shown in Figure 2C and D, respectively.

Quantification of the spectral peaks for cerebral blood and gray matter is shown in Figure 3A along with the time course of the individual quantified spectral peaks. The chemical shifts of both individual spectral peaks over the time-course of the acquisition are shown in Figure 3B. Variation in chemical shift can be observed for the cerebral RBC peak. This indicates underlying variations in the oxygenation of cerebral blood and is used to determine the variation in  $T_1$  associated with it. The time courses of both quantified individual spectral peaks are shown in Figure 3C. Figure 3C also shows the correction to the quantification of the cerebral RBC peak for variation in  $T_1$  of  $^{129}\text{Xe}$  in the RBCs derived using the variation in chemical shift from Figure 3B.

The transfer dynamics of  $^{129}\text{Xe}$  between gray matter and cerebral blood is shown in Figure 4A, both with and without the correction for cerebral blood oxygenation applied to the RBC peak, along with the rescaled and fitted tracer kinetic model from Equation (7) for the tracer transfer constant  $(1 - k) = 0.12$ . Extrapolation of the model to the case of steady-state xenon tissue saturation is shown in Figure 4B, and indicates that the forward transfer ( $T_F$ ) rate of  $^{129}\text{Xe}$  reaches 95% saturation after approximately 200 s. The transfer dynamics of  $^{129}\text{Xe}$

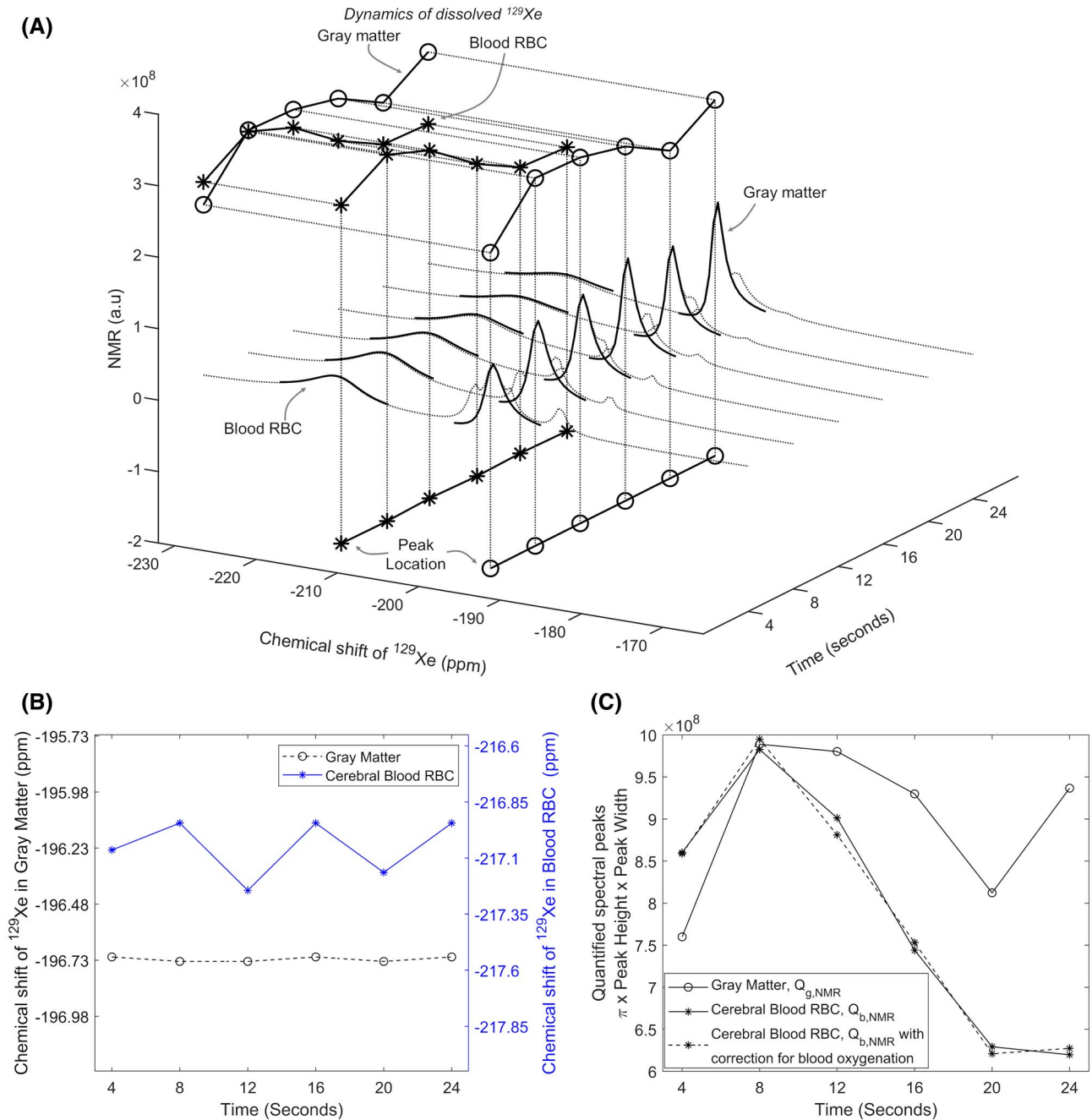


**FIGURE 3** A, Illustration of the quantification and time course of spectral peaks for red blood cells and gray matter. Projection on *Time-chemical shift* plane – time course of the peak location of both spectral peaks. Projection on *Time-NMR unit* plane – time course of both quantified spectral peaks. Note: although peaks were quantified as the product of  $\pi$ , height and width of the peak, only the product of height and width of the peak is shown here for ease of illustration. B, Variation in chemical shift for both peaks; cerebral red blood cells and gray matter. C, Time course of spectral peaks from gray matter and cerebral red blood cells, with and without correction of the RBC peak for variation in  $T_1$  due to blood oxygenation, derived using the variation in chemical shift in (B)

between gray matter and cerebral blood for all the three volunteers for all the three repeats are shown in Figure 5.

For each of the acquisitions, the transfer dynamics with and without the correction for blood oxygenation, along with the variation in chemical shift of  $^{129}\text{Xe}$  in RBCs and the

numerical fit of the tracer kinetic model in Equation (7) are shown. The developed tracer kinetic model returned values for the tracer transfer constant between 0.1 and 0.14 over the three volunteers. The error in the numerical fit was between 2.3% and 4.2% as indicated in Figure 5.

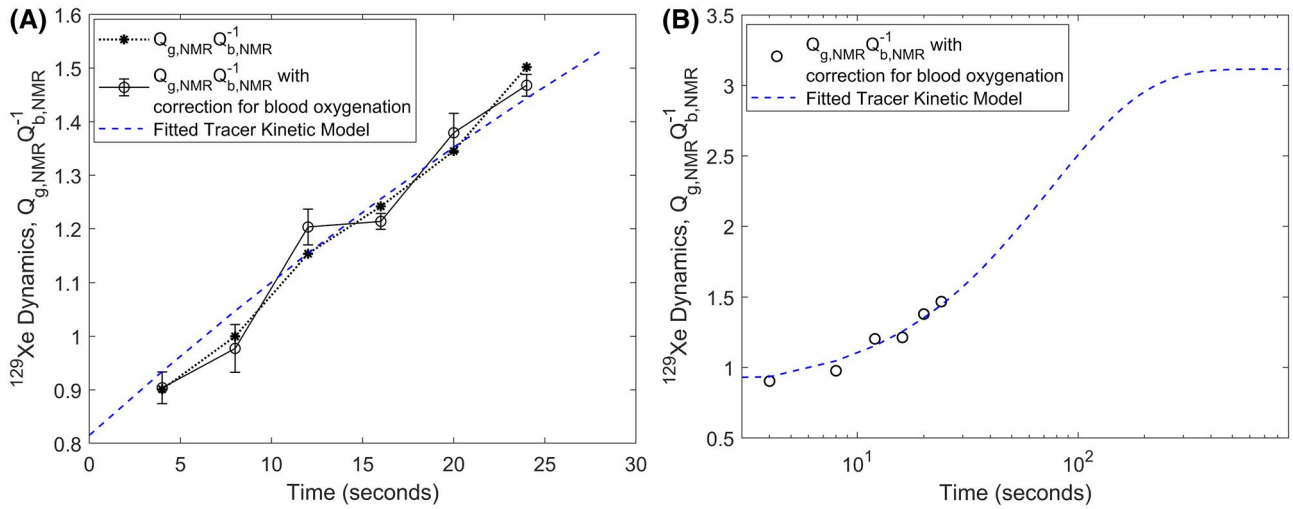


**FIGURE 4** A, Transfer dynamics of  $^{129}\text{Xe}$  between cerebral blood and gray matter, with and without correction of the RBC peak (see Figure 3C), along with a rescaled and fitted tracer kinetic model (from Equation 7) with a tracer transfer constant  $(1-k) = 0.12$ . Error bars calculated considering three repetitions. B, Extrapolation of the tracer kinetic model to illustrate that the *forward transfer* ( $T_F$ ) rate of HP  $^{129}\text{Xe}$  reaches 95% saturation at approximately 200 s

## 5 | DISCUSSION

The unique aspects of the proposed MR spectroscopy technique based on a tracer kinetic model are as follows; First, the dynamics of the relative quantity of  $^{129}\text{Xe}$  is quantified using spectral peaks separated by their distinct chemical shifts, avoiding potential uncertainties related to non-specific binding and partial volume estimates for gray matter and blood which appear to vary with disease progression and aging in the brain.<sup>13,57-60</sup> Second, the NMR signal from the tracer (HP  $^{129}\text{Xe}$ ) once detected after RF excitation becomes NMR invisible ( $DP$ ), enabling the observation of the physiological dynamics of cerebral uptake and diffusional exchange.

An interesting observation of the model is that it predicts that the *forward transfer* ( $T_F$ ) rate ( $M_{GM}M_{Blood}^{-1}$  from Equation 7) increases until saturation. This is because, over time,  $DP$   $^{129}\text{Xe}$  accumulates in the gray matter that will diffuse back (*backward transfer*  $T_B$ ) in to cerebral blood and displace an equal amount of HP  $^{129}\text{Xe}$  (*forward transfer*  $T_F$ ) from cerebral blood to gray matter. This exchange occurs without disrupting the equilibrium in concentration of overall  $^{129}\text{Xe}$  (irrespective of its status of polarization) between the two compartments. In addition, due to continuous arterial blood flow carrying *fresh* HP  $^{129}\text{Xe}$  to the head, the concentration of  $DP$   $^{129}\text{Xe}$  in cerebral blood is much lower than that of gray matter increasing the likelihood of  $DP$   $^{129}\text{Xe}$  in gray matter being replaced by HP  $^{129}\text{Xe}$ . Extrapolation of the model to 200 s and beyond indicates that the model ( $M_{GM}M_{Blood}^{-1}$ ) quickly saturates and is

$\lambda V_{GM} C_A b_{RBC}^{-1} Q_{Blood,HP}^{-1} e^{-\frac{t_{TR}}{T_{1GM}}} e^{\frac{t_{TR}}{T_{1Blood}}} \left(1 - ke^{-\frac{t_{TR}}{T_{VP}}}\right)$  at acquisition  $n = \infty$ . Nevertheless, this saturation time does not have physiological interpretation in the current context.

The factors  $k_1$  and  $k_2$  may not be equal, and estimating these factors individually and their inter-relationship is the scope of future study. The key limitations of the model are that the spectral measurements are performed over the whole brain, and thus average values are considered for cerebral blood flow, cerebral blood volume, mean transit time and gray matter volume. Using spatially resolved spectroscopy and for a known *regional* mean transit time and cerebral blood volume for gray matter, that can be estimated from  $^1\text{H}$  MRI for example,<sup>61</sup> the proposed tracer kinetic model estimates the *regional* efficacy of  $^{129}\text{Xe}$  transfer or uptake across the intact BBB. This might provide additional useful insight in to the underlying *regional* pathophysiology, such as BBB surface area and *intact-barrier* permeability/transferability changes. An in depth clinical investigation of the method in this aspect is the scope of future work. Also, if the mean transit time is known *a priori*, the NMR pulse repetition time can be optimized. Uncertainty in the estimation can be attributed to errors in the numerical fit of the spectra, which in turn can be attributed to the achieved SNR. Future studies will be aided by increases in the signal-to-noise ratio of the spectra, for example by using high-sensitivity radio frequency coils<sup>26</sup> and improved polarization of  $^{129}\text{Xe}$  gas,<sup>53</sup> and these improvements will hopefully facilitate a time-resolved spectroscopic imaging implementation of the global spectroscopy concept proposed here.



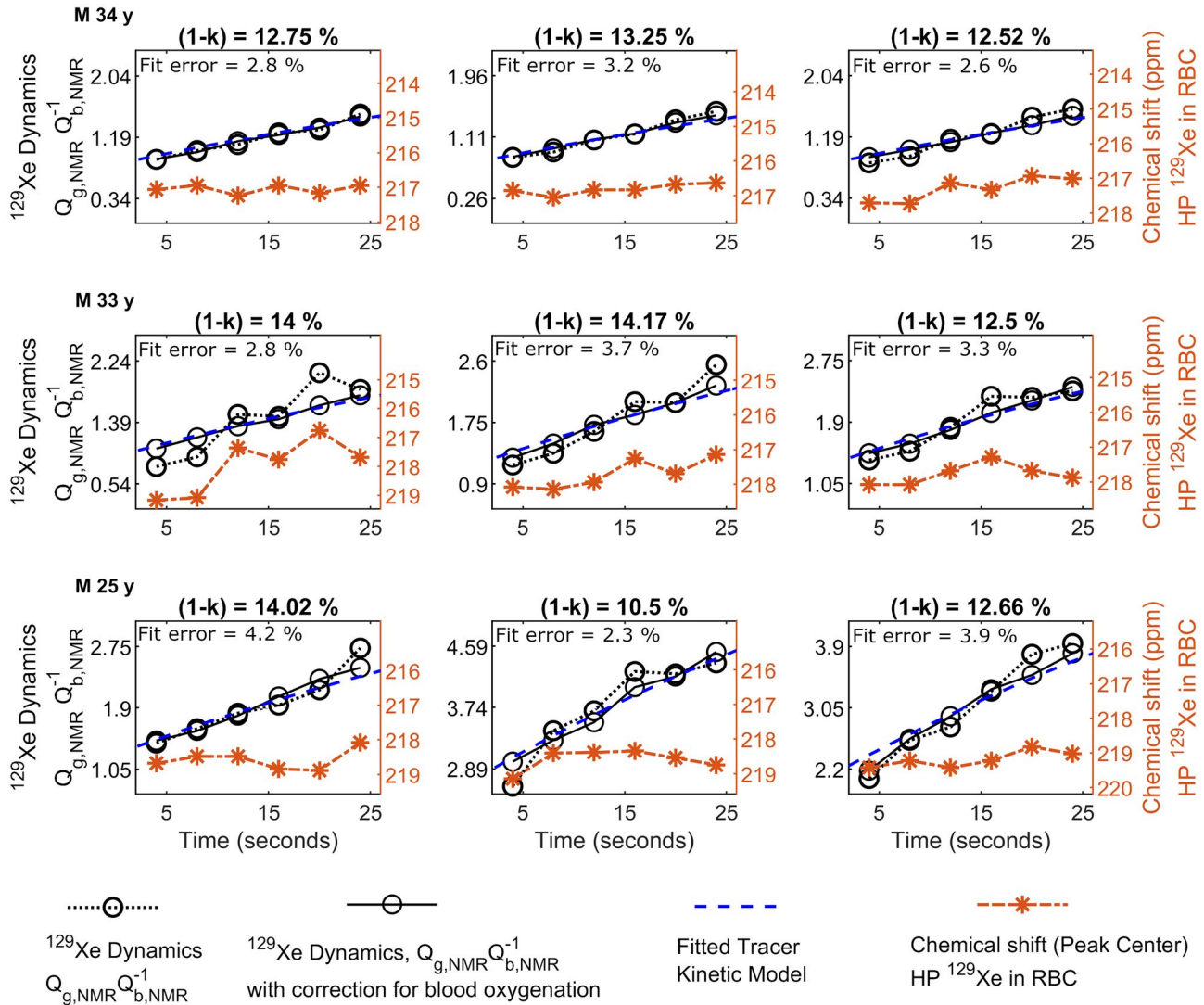


**FIGURE 5** Transfer dynamics with and without correction due to variation in  $T_1$  of red blood cells, along with the rescaled and fitted tracer kinetic model from Equation (7), for three volunteers (rows) and for three separate repetitions (columns). For each of the acquisitions, the variation in chemical shift of  $^{129}\text{Xe}$  in red blood cells is shown. Error in the numerical fit is also indicated


## 6 | CONCLUSIONS

In this study, we developed a tracer kinetic model for time-resolved NMR spectra of HP  $^{129}\text{Xe}$  in the human brain to estimate the transfer rate of HP  $^{129}\text{Xe}$  from cerebral blood to gray matter that depends on a tracer transfer constant for a known mean transit time and cerebral blood volume for gray matter. We believe this model will enable further studies to determine regional  $^{129}\text{Xe}$  tracer transfer constants with a focus of gaining insight into the pathophysiology of the BBB in diseases such as intact-barrier edema, arterial plaque, inflammation, infarct following stroke and to aid the assessment of drug delivery to the brain. In addition, in light of the passive nature of the xenon tracer, it could serve as a cross-reference for studies involving oxygen, water or glucose uptake, which are driven by metabolism and/or electrolytic balance.

## ACKNOWLEDGMENTS

Funding from MRC grant MR/M008894/1. Authors acknowledge Paul D Griffiths and Nigel Hoggard for useful discussions about brain physiology.

## ORCID

Madhwesha R. Rao  <https://orcid.org/0000-0002-4109-4176>

Graham Norquay  <https://orcid.org/0000-0002-4108-9035>

Neil J. Stewart  <https://orcid.org/0000-0001-8358-394X>

Jim M. Wild  <https://orcid.org/0000-0002-7246-8660>

## TWITTER

Madhwesha R. Rao  @Madhwesha

## REFERENCES

1. Abbott NJ, Patabendige AA, Dolman DE, Yusof SR, Begley DJ. Structure and function of the blood-brain barrier. *Neurobiol Dis.* 2010;37:13-25.
2. Wintermark M, Sesay M, Barbier E, et al. Comparative overview of brain perfusion imaging techniques. *Stroke.* 2005;36:e83-e99.
3. Albers GW. Diffusion-weighted MRI for evaluation of acute stroke. *Neurology.* 1998;51(Suppl 3):S47-S49.
4. Brindle KM, Izquierdo-Garcia JL, Lewis DY, Mair RJ, Wright AJ. Brain Tumor Imaging. *J Clin Oncol.* 2017;35:2432-2438.
5. Burghart G, Finn CA. *Handbook of MRI scanning - E-Book.* Amsterdam, Netherlands: Elsevier Health Science; 2012.
6. Jack CR Jr, Bernstein MA, Fox NC, et al. The Alzheimer's disease neuroimaging initiative (ADNI): MRI methods. *J Magn Reson Imaging.* 2008;27:685-691.
7. Jack CR Jr, Bennett DA, Blennow K, et al. NIA-AA research framework: toward a biological definition of Alzheimer's disease. *Alzheimers Dement.* 2018;14:535-562.
8. Pham-Huy LA, He H, Pham-Huy C. Free radicals, antioxidants in disease and health. *Int J Biomed Sci.* 2008;4:89-96.
9. Huang W-J, Zhang X, Chen W-W. Role of oxidative stress in Alzheimer's disease. *Biomed Rep.* 2016;4:519-522.
10. Bell RD, Winkler EA, Sagare AP, et al. Pericytes control key neurovascular functions and neuronal phenotype in the adult brain and during brain aging. *Neuron.* 2010;68:409-427.
11. Poon HF, Calabrese V, Scapagnini G, Butterfield DA. Free radicals and brain aging. *Clin Geriatr Med.* 2004;20:329-359.
12. Heye AK, Culling RD, Valdés Hernández MDC, Thrippleton MJ, Wardlaw JM. Assessment of blood-brain barrier disruption using dynamic contrast-enhanced MRI. A systematic review. *Neuroimage Clin.* 2014;6:262-274.
13. Koenig M, Klotz E, Luka B, Venderink DJ, Spittler JF, Heuser L. Perfusion CT of the brain: diagnostic approach for early detection of ischemic stroke. *Radiology.* 1998;209:85-93.
14. Miles KA, Griffiths MR. Perfusion CT: a worthwhile enhancement? *Br J Radiol.* 2003;76:220-231.
15. von Kummer R, Allen KL, Holle R, et al. Acute stroke: usefulness of early CT findings before thrombolytic therapy. *Radiology.* 1997;205(2):327-333.
16. Gillard JH, Waldman AD, Barker PB. *Clinical MR Neuroimaging: Physiological and Functional Techniques.* Cambridge, UK: Cambridge University Press; 2009.
17. Williams DS, Detre JA, Leigh JS, Koretsky AP. Magnetic resonance imaging of perfusion using spin inversion of arterial water. *Proc Natl Acad Sci USA.* 1992;89:212-216.
18. Detre JA, Zhang W, Roberts DA, et al. Tissue specific perfusion imaging using arterial spin labeling. *NMR Biomed.* 1994;7(2):75-82.
19. Alsop DC, Detre JA, Golay X, et al. Recommended implementation of arterial spin-labeled perfusion MRI for clinical applications: a consensus of the ISMRM perfusion study group and the European consortium for ASL in dementia. *Magn Reson Med.* 2015;73:102-116.
20. Wang DJJ, Alger JR, Qiao JX, et al. Multi-delay multi-parametric arterial spin-labeled perfusion MRI in acute ischemic stroke - comparison with dynamic susceptibility contrast enhanced perfusion imaging. *Neuroimage Clin.* 2013;3:1-7.
21. Ohene Y, Harrison IF, Nahavandi P, et al. Non-invasive MRI of brain clearance pathways using multiple echo time arterial spin labelling: an aquaporin-4 study. *NeuroImage.* 2019;188:515-523.
22. Shao X, Ma SJ, Casey M, D'Orazio L, Ringman JM, Wang DJJ. Mapping water exchange across the blood-brain barrier using 3D diffusion-prepared arterial spin labeled perfusion MRI. *Magn Reson Med.* 2019;81:3065-3079.
23. Schidlowski M, Boland M, Rüber T, Stöcker T. Blood-brain barrier permeability measurement by biexponentially modeling whole-brain arterial spin labeling data with multiple T2-weightings. *NMR Biomed.* 2020;33:e4374.
24. Niibo T, Ohta H, Miyata S, Ikushima I, Yonenaga K, Takeshima H. Prediction of blood-brain barrier disruption and intracerebral hemorrhagic infarction using arterial spin-labeling magnetic resonance imaging. *Stroke.* 2017;48:117-122.
25. Buxton RB, Frank LR, Wong EC, Siewert B, Warach S, Edelman RR. A general kinetic model for quantitative perfusion imaging with arterial spin labeling. *Magn Reson Med.* 1998;40:383-396.
26. Rao MR, Stewart NJ, Griffiths PD, Norquay G, Wild JM. Imaging human brain perfusion with inhaled hyperpolarized (<sup>129</sup>Xe) MR imaging. *Radiology.* 2018;286:659-665.
27. Rao M, Stewart NJ, Norquay G, Griffiths PD, Wild JM. High resolution spectroscopy and chemical shift imaging of hyperpolarized (<sup>129</sup>Xe) dissolved in the human brain in vivo at 1.5 tesla. *Magn Reson Med.* 2016;75(6):2227-2234.
28. Rao M, Norquay G, Wild JM. Assessment of repeatability of imaging inhaled hyperpolarized xenon-129 in the human brain. *Proc Intl Soc Mag Reson Med.* 2019;27:3319.
29. Rao MR, Norquay G, Stewart NJ, Hoggard N, Griffiths PD, Wild JM. Assessment of brain perfusion using hyperpolarized <sup>129</sup>Xe MRI in a subject with established stroke. *Journal of Magnetic Resonance Imaging.* 2019;50:1002-1004.
30. Hane FT, Li T, Plata J-A, Hassan A, Granberg K, Albert MS. Inhaled xenon washout as a biomarker of Alzheimer's disease. *Diagnostics.* 2018;8:41.
31. Shepelytskyi Y, Hane FT, Grynko V, Li T, Hassan A, Albert MS. Hyperpolarized <sup>129</sup>Xe time-of-flight MR imaging of perfusion and brain function. *Diagnostics.* 2020;10:630.
32. Norquay G, Leung G, Stewart NJ, Tozer GM, Wolber J, Wild JM. Relaxation and exchange dynamics of hyperpolarized (<sup>129</sup>Xe) in human blood. *Magn Reson Med.* 2015;74:303-311.
33. Walker TG, Happer W. Spin-exchange optical pumping of noble-gas nuclei. *Rev Mod Phys.* 1997;69:629-642.
34. Peled S, Jolesz FA, Tseng CH, Nascimben L, Albert MS, Walsworth RL. Determinants of tissue delivery for Xe-129 magnetic resonance in humans. *Magn Reson Med.* 1996;36:340-344.
35. Martin CC, Williams RF, Gao JH, Nickerson LDH, Xiong JH, Fox PT. The pharmacokinetics of hyperpolarized xenon: Implications for cerebral MRI. *JMRI-J Magn Reson Imaging.* 1997;7:848-854.
36. Kilian W, Seifert F, Rinneberg H. Dynamic NMR spectroscopy of hyperpolarized <sup>129</sup>Xe in human brain analyzed by an uptake model. *Magn Reson Med.* 2004;51:843-847.
37. Kandel E, Schwartz JH, Jessell T. *Principles of Neural Science.* New York City, USA: McGraw-Hill Medical; 2000.
38. Leenders KL, Perani D, Lammertsma AA, et al. Cerebral blood flow, blood volume and oxygen utilization: normal values and effect of age. *Brain.* 1990;113:27-47.
39. Rengachary SS, Ellenbogen RG. *Principles of Neurosurgery.* Maryland Heights, USA: Elsevier Mosby; 2005.

40. Duelli R, Kuschinsky W. Changes in brain capillary diameter during hypocapnia and hypercapnia. *J Cereb Blood Flow Metabol.* 1993;13:1025-1028.
41. Duvernoy H, Delon S, Vannson JL. The vascularization of the human cerebellar cortex. *Brain Res Bull.* 1983;11:419-480.
42. Nicholson CP. Diffusion and related transport mechanisms in brain tissue. *Rep Prog Phys.* 2001;64:815-884.
43. Wong AD, Ye M, Levy AF, Rothstein JD, Bergles DE, Searson PC. The blood-brain barrier: an engineering perspective. *Front Neuroeng.* 2013;6:7.
44. Wise DL, Houghton G. Diffusion coefficients of neon, krypton, xenon, carbon monoxide and nitric oxide in water at 10-60°C. *Chem Eng Sci.* 1968;23:1211-1216.
45. Kety SS. The theory and applications of the exchange of inert gas at the lungs and tissues. *Pharmacol Rev.* 1951;3:1-41.
46. Ibaraki M, Ito H, Shimosegawa E, et al. Cerebral vascular mean transit time in healthy humans: a comparative study with PET and dynamic susceptibility contrast-enhanced MRI. *J Cereb Blood Flow Metab.* 2007;27:404-413.
47. Blinkov SM. *The Human Brain in Figures and Tables: A Quantitative Handbook.* Basic Books; 1968.
48. Haacke EM, Brown RW, Thompson MR, Venkatesan R. *Magnetic Resonance Imaging: Physical Principles and Sequence Design.* Wiley; 1999.
49. De Graaf RA. *In Vivo NMR Spectroscopy: Principles and Techniques.* Chichester, UK: John Wiley & Sons; 2019.
50. Norquay G, Leung G, Stewart NJ, Wolber J, Wild JM. <sup>129</sup>Xe chemical shift in human blood and pulmonary blood oxygenation measurement in humans using hyperpolarized <sup>129</sup>Xe NMR. *Magn Reson Med.* 2017;77:1399-1408.
51. Wolber J, Cherubini A, Dzik-Jurasz AS, Leach MO, Bifone A. Spin-lattice relaxation of laser-polarized xenon in human blood. *Proc Natl Acad Sci USA.* 1999;96(7):3664-3669.
52. Albert MS, Balamore D, Kacher DF, Venkatesh AK, Jolesz FA. Hyperpolarized <sup>129</sup>Xe T1 in oxygenated and deoxygenated blood. *NMR Biomed.* 2000;13:407-414.
53. Norquay G, Collier GJ, Rao M, Stewart NJ, Wild JM. <sup>129</sup>Xe-Rb spin-exchange optical pumping with high photon efficiency. *Phys Rev Lett.* 2018;121:153201.
54. Qing K, Ruppert K, Jiang Y, et al. Regional mapping of gas uptake by blood and tissue in the human lung using hyperpolarized xenon-129 MRI. *J Magn Reson Imaging: JMRI.* 2014;39:346-359.
55. Laitio RM, Kaisti KK, Langsjo JW, et al. Effects of xenon anesthesia on cerebral blood flow in humans - a positron emission tomography study. *Anesthesiology.* 2007;106:1128-1133.
56. Meyer JS, Hayman LA, Amano T, et al. Mapping local blood-flow of human-brain by CT scanning during stable xenon inhalation. *Stroke.* 1981;12:426-436.
57. González Ballester MÁ, Zisserman AP, Brady M. Estimation of the partial volume effect in MRI. *Med Image Anal.* 2002;6:389-405.
58. Soret M, Bacharach SL, Buvat I. Partial-volume effect in PET tumor imaging. *J Nucl Med.* 2007;48:932-945.
59. Tang C, Blatter DD, Parker DL. Accuracy of phase-contrast flow measurements in the presence of partial-volume effects. *J Magn Reson Imaging.* 1993;3:377-385.
60. Matsuda H, Ohnishi T, Asada T, et al. Correction for partial-volume effects on brain perfusion SPECT in healthy men. *J Nucl Med.* 2003;44:1243-1252.
61. Rao M, Norquay G, Wild JM. Investigating gas-exchange and tissue perfusion in the human brain using a combination of proton and hyperpolarized xenon-129 MRI. *Proc Intl Soc Mag Reson Med.* 2019;27:3095.

**How to cite this article:** Rao MR, Norquay G, Stewart NJ, Wild JM. Measuring <sup>129</sup>Xe transfer across the blood-brain barrier using MR spectroscopy. *Magn Reson Med.* 2021;85:2939–2949. <https://doi.org/10.1002/mrm.28646>